Talanta 85 (2011) 1560–1565

Contents lists available at ScienceDirect

Talanta

journal homepage: www.elsevier.com/locate/talanta

Development of interdigitated arrays coated with functional polyaniline/MWCNT for electrochemical biodetection: Application for human papilloma virus

Lam Dai Tran[a,*], Dzung Tuan Nguyen[b], Binh Hai Nguyen[a], Quan Phuc Do[c], Huy Le Nguyen[d]

[a] Institute of Materials Science, Vietnam Academy of Science and Technology, 18 Hoang Quoc Viet Road, Ha Noi, Viet Nam
[b] Institute for Tropical Technology, Vietnam Academy of Science and Technology, 18 Hoang Quoc Viet Road, Ha Noi, Viet Nam
[c] Research Center for Environmental Technology and Sustainable Development, Hanoi University of Science, 354 Nguyen Trai Road, Ha Noi, Viet Nam
[d] School of Chemical Engineering, Hanoi University of Science and Technology, 1 Dai Co Viet Road, Ha Noi, Viet Nam

ARTICLE INFO

Article history:
Received 20 April 2011
Received in revised form 16 June 2011
Accepted 16 June 2011
Available online 23 June 2011

Keywords:
Interdigitated arrays (IDA)
Polyaniline-multiwalled carbon nanotube film (PANi–MWCNT)
Peptide aptamer-antigen affinity
Electrochemical detection
Human papilloma virus (HPV)

ABSTRACT

In this study, polyaniline-multiwalled carbon nanotube film (PANi–MWCNT) has been polymerized on interdigitated platinum electrode arrays (IDA), fabricated by MEMS technology for the detection of human papillomavirus (HPV) infection, using immobilized peptide aptamers as affinity capture reagent. Label-free, electrochemical detection of the specific immune reaction between antigen peptide aptamer HPV-16-L1 (with a molecular weight of 1825 Da), the most common genotype in cytological normal women worldwide, and its specific antibody of HPV-16 (which is much bigger with molecular weight of ca. 150 kDa) on multifunctional PANi–MWCNT based arrays was reported. The most significant advantage of this technique consists of reagentless and multiple detection of antigen–antibody complex formation on well conducting IDA interface of PANi–MWCNT, without intermediate steps or any labeling reagents, as normally required in the previous works.

1. Introduction

Cancer of the cervix is the third most common cancer in women worldwide with an estimated 529,000 new cases in 2008 [1]. The role of human papilloma virus (HPV) in the etiology of cervical cancer precursor lesions and invasive carcinoma development has been well established. It is a member of the papilloma virus family of viruses that is capable of infecting humans. Like all papilloma viruses, HPVs establish productive infections only in the stratified epithelium of the skin or mucous membranes. While the majority of the nearly 200 known types of HPV cause no symptoms in most people, some types can cause warts (verrucae), while others can – in a minority of cases – lead to cancers of the cervix, vulva, vagina, and anus in women or cancers of the anus and penis in men. Infection with high-risk HPV types is associated with the development of cervical cancer, currently the second most common cancer among women worldwide. The most common high-risk or oncogenic HPV types are HPV-16 and HPV18 [2–8]. These facts showed the importance in detecting the presence of anti-HPV antibody response in sexual active young people. Until now, most of serological analyses, either in case of natural infection or in prophylactic vaccines have relied on enzyme-linked immunosorbent assays (ELISAs) [9]. Owing to the difficulties to perform serological assays and HPV cultures efficiently, some tools based on molecular recognition have been developed for the diagnosis of HPV infections. At the basis of molecular recognition, the detection of HPV DNA are in use, based on the extraction of genomic DNA from clinical samples with posterior PCR amplification and detection. However, due to the high mutation rates of viruses, detection by PCR is complicated [10].

Electrochemical biosensors have received considerable attention regarding the detection of DNA hybridization due to the advantages of low cost, simplicity, high sensitivity, compatibility with mass manufacturing, possibility of microfabrication technologies and portability, making them excellent candidates for point-of-care DNA diagnostics. Electrochemical detection of HPV related sequences has been reported in the past by using methylene-blue as hybridization indicator or secondary probes labeled with ferrocene [11]. In the first case, a 20-mer probe sequence was adsorbed on the surface of a graphite electrode and used for the detection of a 20-mer target related to L1 gene of identical length by recording the variations in methylene-blue response before and after target recognition, achieving a limit of detection of 1.2 ng/μL (0.5 nM). The other example involved the use of a bioelectronic DNA detection platform formerly commercialized as eSensor™, for the detection of HPV sequences based on thiolated probes immobilized on the chip surface. After target

* Corresponding author. Tel.: +84 4 37564129; fax: +84 4 38360705.
E-mail address: lamtd@ims.vast.ac.vn (L.D. Tran).

0039-9140/$ – see front matter © 2011 Elsevier B.V. All rights reserved.
doi:10.1016/j.talanta.2011.06.048

immobilization, a ferrocene-labeled probe was hybridized and the current response was measured. These chips were able to detect 86% of the HPV targets contained in clinical samples using a positive/negative type response. In a more recent report, detection of HPV was carried out by treating a captured dsDNA duplex with acid and directly measuring the released purine bases by square wave voltammetry [12]. An electrochemical sensor microarray based on DNA detection for the individual and simultaneous detection of specific high-risk HPV sequences, more specifically HPV-16 and 45 and analytical parameters such as sensitivity, specificity and reproducibility have been studied [13].

The primary objective of this work is to design a sensitive interface for electrochemically multiplexed analyses of biomolecules. Several advantageous features of this platform will be developed. First, IDA is attractive for their possibility to eliminate the main drawbacks of the electrochemical sensors such as the phenomenon of "electrode fouling", the "memory effect" from one sample to another as well as the possibility to be produced inexpensively at large scale. Second, designed hybrid organic–inorganic electrode interface is expected to express a synergic effect to the overall system and thus improve sensing characteristics. Actually, some metal oxide nanoparticles such as iron oxide (Fe_3O_4), zinc oxide (ZnO) and especially carbon nanotube (CNT) and graphene having a large surface-to-volume ratio, high surface reaction activity, high catalytic efficiency and strong adsorption ability were proved to be useful for improving sensor stability and sensitivity [14–16]. In this study, a specific peptide aptamer as probe was used to target HPV. Peptide aptamers belong to a promising class of affinity reagents that can be used to bind target proteins and dissect biological processes. These reagents generally comprise proteins that have been engineered to mimic antibodies by displaying loops or surfaces that specifically bind a target protein. Effectively, it has been shown that the 15 amino acid HPV-16-L1 peptide aptamer (311–325 sequence, Asn–Leu–Ala–Ser–Ser–Asn–Tyr–Phe–Pro–Thr–Pro–Ser–Gly–Ser–Met), being a part of the HPV-16 virus capside, is specifically recognized by antibodies directed against the HPV-16 virus itself. This approach was first proposed by Piro et al. [17].

For IDA platform, multifunctional PANi–MWCNT composite film was elaborated. Then, HPV-16-L1 (with a molecular weight of 1825 Da) was grafted as probe to detect the HPV-16 antibody (Ab) (which is much bigger (ca. 150 kDa) than the peptide aptamer probe). It is therefore expected that the presence of the peptide aptamer/Ab complex in the vicinity of the polymer/solution interface strongly influences the electroactivity and switching rate of the conducting polymer, so that a current change could be detected after recognition of antigen–antibody, in a direct and label-free detection format. The significant advantage of this technique consists of reagentless and multiple detection of antigen–antibody complex formation on well conducting IDA interface of PANi–MWCNT, without intermediate steps or any labeling reagents, as normally required in the previous works.

2. Experimental

2.1. Chemical and biochemical reagents

N′-(3-dimethylaminopropyl)-N-ethylcarbodiimide hydrochloride (EDC), N-hydroxysuccinimide (NHS) were provided by Sigma. Aqueous solutions were made with DI water (18 MΩ). Carboxylic mutilwall carbon nanotube (MWCNTc) was purchased from Shenzhen Nanotech Port Co., Ltd., China (purity CNTs > 98%, out diameter: 10–20 nm, length: 5–15 μm, carboxyl ratio: 2.31 wt%). Aniline (Merck, 99.5%) was distilled under vacuum prior to polymerization. OVA (egg albumin, 2× crystallized) was purchased from Calbiochem, La Jolla, CA, USA. HPV-16-L1 peptide (311–325 sequence, i.e. Asn–Leu–Ala–Ser–Ser–Asn–Tyr–Phe–Pro–Thr–Pro–Ser–Gly–Ser–Met) was purchased from Genscript, USA. Secondary goat $F(ab')_2$ anti-mouse Ig conjugated to horseradish peroxidase was purchased from Tebu (Le Perray-en-Yvelines, France). Antibodies against HPV (anti HPV, mouse anti-papillomavirus 16 L1 late protein, monoclonal antibody) and against Ovalbumin (anti-Ovalbumin, anti-OVA) were obtained from AbD serotec (Morphosys, UK).

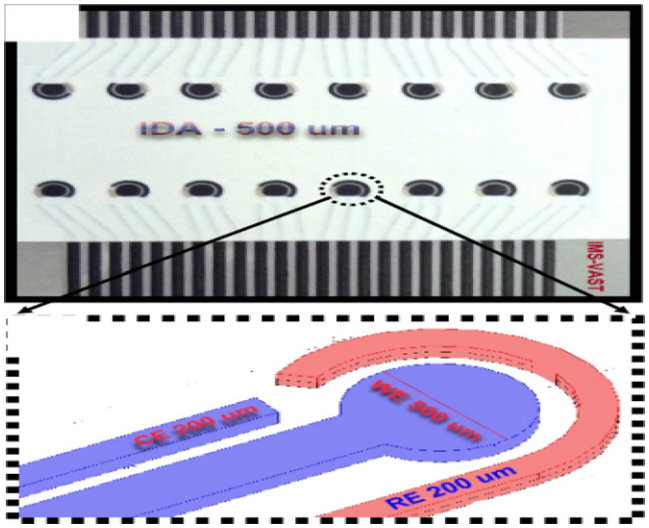

Fig. 1. Schematic representation of IDA electrodes.

2.2. Interdigitated arrays fabrication

The interdigitated arrays (IDA) as shown in Fig. 1 were fabricated on silicon substrate via lithography technique. Silicon wafers were covered with a layer of SiO_2 1 μm thick by means of dry thermal oxidation. The wafer was spin-coated with a layer of photoresist AZ5214E (1 μm thickness) and the shape of the electrodes was defined by UV-photolithography. Then, chromium and platinum were sputtered on the top of the wafer with the thickness of 50 and 500 nm, respectively. The working and counter electrodes were patterned by a lift-off process (30 s in acetone solution with ultrasonic vibration). A second photolithographic step is carried out to deposit the silver layer. Next, a 50 mM solution of $FeCl_3$ (Merck) was applied to the silver surface for 50 s at room temperature, followed by rinsing with DI water to define the reference electrodes. The final diameter of the working electrodes was 500 μm.

2.3. Electropolymerization of PANi–MWCNT film

The PANi–MWCNT film was electropolymerized on IDA using cyclic voltammetry within the potential range from −0.2 to +1.0 V (vs. SCE) with sweep rate of 50 mV/s, in a fresh solution containing 0.1 M ANi in 0.5 M H_2SO_4 and 0.8 wt% MWCNTc (weight percent with respect to ANi).

2.4. Peptide aptamer grafting and peptide–antibody reaction conditions

For HPV-16-L1 grafting, 1.5×10^{-4} M EDC + 3×10^{-4} M NHS were prepared with ultra-pure water. Then 50 nM HPV-16-L1 was added. PANi–MWCNT electrodes were put into this solution during 2 h under stirring at 37 °C. Afterwards, the electrode was rinsed in water during 30 min under stirring at 37 °C.

For immune reaction between the peptide aptamer and the antibody, a concentration range from 10 to 50 nM (in DI water) of

anti-HPV was used in our tests. The electrodes pre-modified with HPV-16-L1 aptamer were left to react with anti-HPV for 15 min, under stirring at 37 °C, and then thoroughly washed in water under stirring at the same temperature. As for blank experiment with irrelevant antibodies (anti-OVA and/or anti- Keyhole Limpet Hemocyanin, anti-KLH) the same conditions were applied.

2.5. Electrochemical measurements

Voltammetric measurements were performed on AUTOLAB PGSTAT 30 Electrochemical Analyser (EcoChemie, the Netherlands) under the control of GPES software (ver. 4.9). The parameters for CV: scan rate: 50 mV/s; potential range of −0.5 to 0.6 V vs. SCE. The parameters for SWV were optimized as follows: frequency: 12.5 Hz; start potential: −0.5 V; end potential: +0.5 V; step: 8 mV; amplitude: 25 mV. Prior to SWV measurements, the electrodes were held for 120 s at the starting potential for conditioning. The SWV scans were repeated until complete stabilization of the electrochemical signal (i.e., no difference observed between two successive responses). All electrochemical experiments were conducted at room temperature.

3. Results and discussion

3.1. Electrochemical synthesis of PANi–MWCNT composite

The cyclic voltammograms (CVs) recorded during 20-cycle synthesis of PANi–MWCNT are shown in Fig. 2a. The oxidation peaks at about 0.16 V are related to the transformation of PANi from leucoemeraldine form (fully reduced state) to emeraldine salt (neutral state). The small oxidation peaks at about 0.4 V are due to the branched structure of PANi–MWCNT layers. The oxidation peaks at about 0.62 V refer to the state transformation from emeraldine to pernigraniline (fully oxidized state). The peak current increase of the two main oxidation peaks at about 0.16 and 0.62 V indicates that well conducting PANi film has been formed. It can be seen from Fig. 2b that under the same experimental conditions, the current peak of PANi–MWCNT was almost 4 times larger than that of pure PANi after 20 cycle formation, which confirms well the role of CNT in increasing composite conductivity as well as its surface area, two main parameters that can significantly improve the overall biosensor performance.

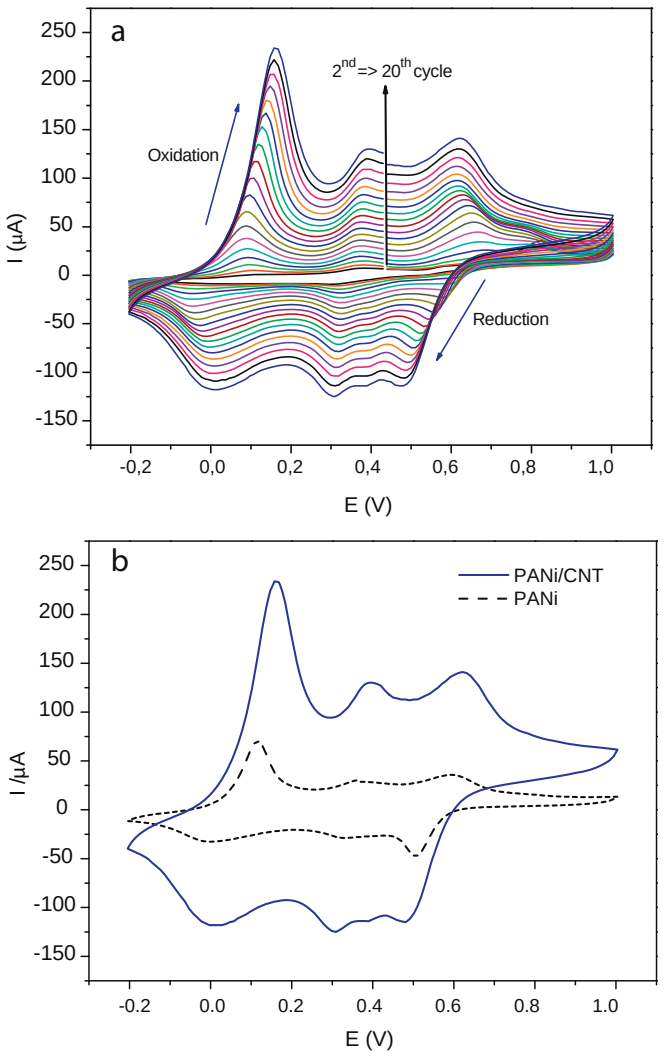

Fig. 2. Electropolymerization of PANi–MWCNT (a) and CVs comparison of PANi film with PANi–MWCNT composite during electropolymerization (b).

3.2. PANi–MWCNT composite characterization

FE-SEM image revealed that PANi–MWCNT composite consists of porous networks formed by MWCNT and PANi (Fig. 3a). Being uniform and porous, this structure is well suitable for biocomponent immobilization.

The roughness of the surface of PANi–MWCNT composite was characterized by using AFM techniques (Fig. 3b). AFM image showed that the surface of composite was porous with roughness about 0.33 μm; this means the active area of composite was larger than PANi films and absorption ability was increased.

The FTIR spectrum of PANi–MWCNT composite (Fig. 4, solid curve) presents benzenoid (B) and quinoid (Q) ring stretching bands (C=C) appeared at 1460 and 1612 cm^{-1}. The peaks at 1110 and 3415 cm^{-1} can be attributed to $B{=}N^{+}{=}Q$ stretching and –N–H stretching vibrations respectively of PANi in the composite film. The peak at 1702 cm^{-1} is unambiguously attributed to $–COO^{-}$ stretching vibration, clearly indicating the presence of carboxyl group (–COOH) [22]. This fingerprint vibration of –COOH group is very important for successful immobilization of HPV-16-L1 aptamer via amine coupling, using the most common approach with aqueous mixture of EDC/NHS groups to yield amine reactive esters. While in the pure PANi the intensity of the quinonoid band is obviously higher than that of benzenoid band (meaning that PANi is richer in quinonoid unit (dotted line), i.e. Q/B > 1), in the PANi–MWCNT the ratio of Q/B decreases (intensity of the quinonoid band is reduced), which can be explained by the fact that MWCNT interacts strongly with the conjugated structure of PANi, especially via quinonoid unit.

3.3. HPV-16-L1 aptamer grafting on PANi–MWCNT composite

As discussed above, peptide aptamer, made of a few amino acids, can bind antibodies with high affinity (K_d 10^6–10^9 M) [18–23]. They are commonly used in ELISA and biosensors as they are more stable, safer to handle, more available than viral proteins or cells and moreover can be designed and synthesized on purpose. In our study, HPV-16-L1 was grafted onto PANi–MWCNT coated IDA as described in Section 2. The immobilization was a determinant step in the electrochemical biosensor fabrication. HPV-16-L1 is a small peptide with a molecular weight of 1825 Da therefore can be immobilized without a significant hinderance of the electrode surface (i.e. does not produce a complete surface blockage for ion transport into the polymer film), providing that it is grafted at relatively low surface densities.

Next, the antibody molecule (ca. 150 kDa for anti-HPV, as it is an IgG one) is much bigger and more voluminous than HPV-16-L1

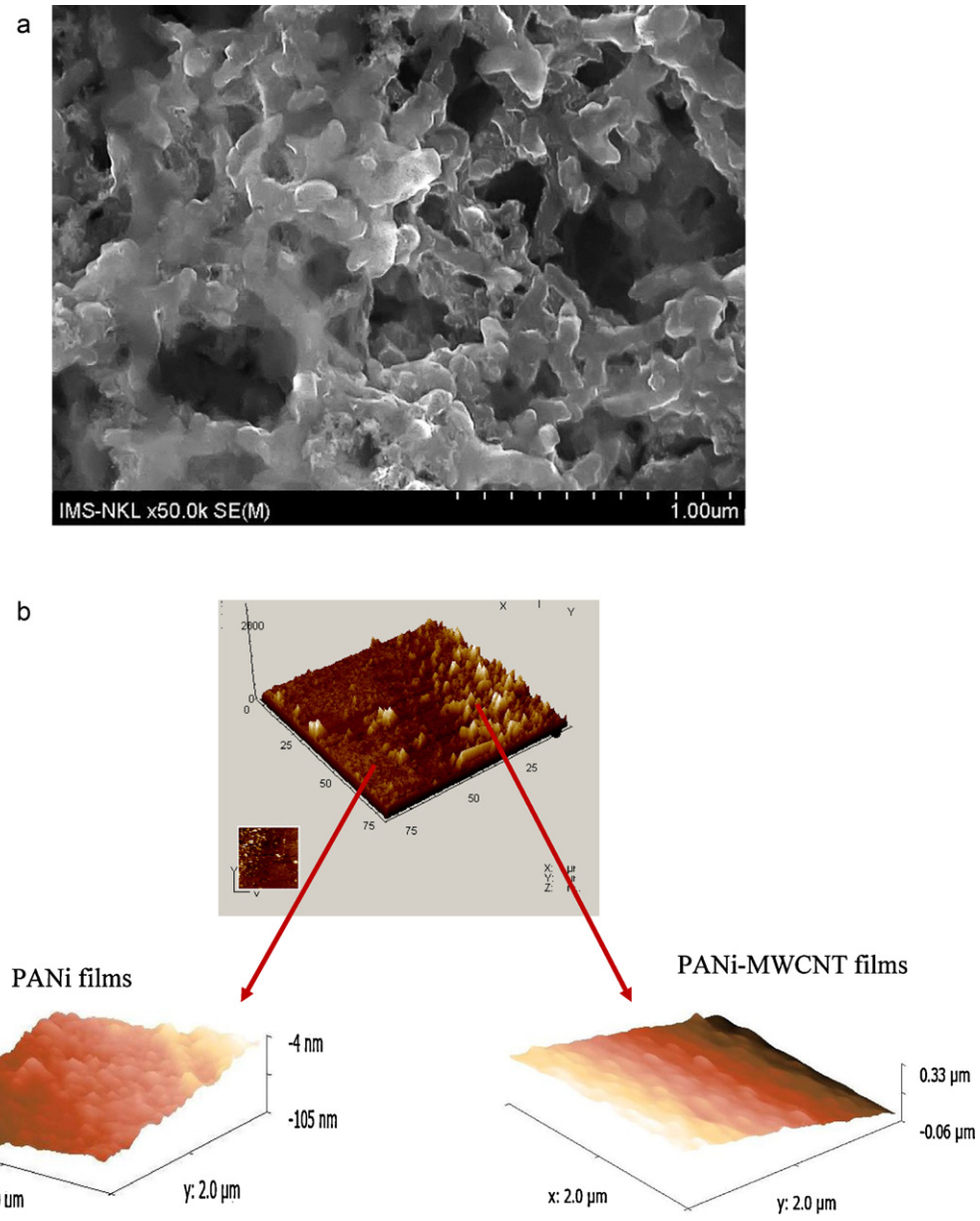

Fig. 3. FE-SEM image (a) and AFM image (b) of PANi–MWCNT film.

probe. The average surface occupied by one anti-HPV-16 antibody molecule could be estimated as ca. 10^4 Å^2 [17]. Therefore, the surface of anti-HPV-16 molecules available to form a uniform blocking layer on the polymer surface would be as low as ca. 15 pmol cm^{-2}.

On the basis of this estimation, HPV-16-L1 was grafted at low surface density (i.e. at 50 nmol L^{-1} or lower, 50 nmol L^{-1} is the concentration than was normally used in spectrophotometric assays [17]). This HPV-16-L1 density would warrant an efficient complete immune reaction between HPV-16-L1 and anti-HPV-16. Effectively, 0.1 nmol L^{-1} HPV-16-L1 will induce negligible SWV signal after grafting, whereas for 1 μmol L^{-1} HPV-16-L1 and higher, a full surface blockage is achieved and subsequent complexation cannot be detected by SWV (results not shown).

As shown in Fig. 5, the cyclic voltammogram shows two wave pairs at −0.25 V/−0.28 V and +0.1 V/−0.01 V. As it is the faradic component, which is relevant to characterize diffusion hindering, square wave voltammetry has been advantageously used in the following experiments, instead of classical cyclic voltammetry. The SWV choice instead of CV is rationalized on its ability to reduce capacitive current as well as the parasite current due to reduction of dissolved oxygen (in SWV, the currents are sampled in both positive and negative pulses successively, furthermore, the registered current is the subtraction between oxidation and reduction currents, thus current density in SWV's are higher that those in CVs, recorded for the same electrode [24]).

3.4. Electrochemical detection of HPV-16-L1 aptamer:anti HPV complex

SWV obtained before and after grafting of HPV-16-L1 were clearly shown in Fig. 6 (curve 1 and curve 2, respectively). Further, with the use of SWV we could demonstrate the presence of complex formation between HPV-16-L1 aptamer and its specific (relevant) anti-HPV. As expected, formation of the HPV-16-L:anti-HPV-16 complex induces significant current drops (Fig. 6, curves 3–7, depending on added anti-HPV-16 concentration). Furthermore, it is possible to perform decomplexation followed by re-complexation

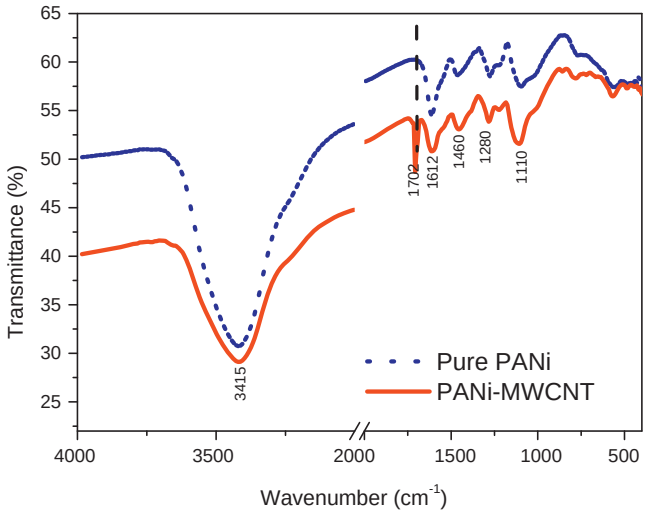

Fig. 4. FTIR spectra of PANi and PANi–MWCNT composite.

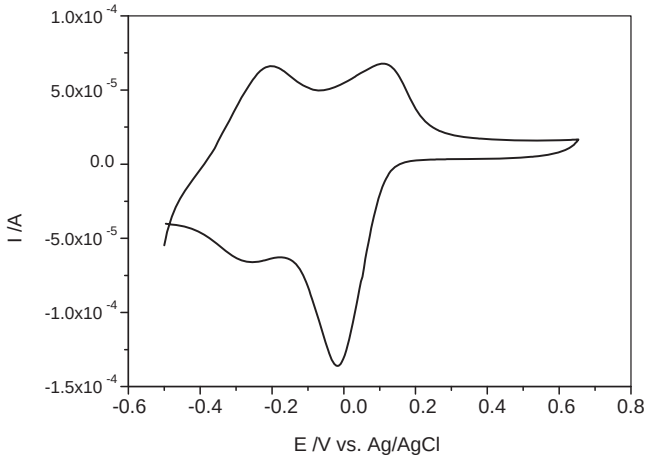

Fig. 5. Electroactive CV of PANi–MWCNT composite in 0.1 M HCl. $v = 50$ mV/s.

and so on for at least 5 times, thus indicating the reversibility of Ag–Ab interaction as well as the robustness of this IDA based arrays.

To evaluate the analytical performance of above IDA arrays, a calibration curve was done for a series of anti-HPV-16 concentration ranging from 10 to 80 nM. As it can be seen, the signal tends to saturation for concentrations above 80 nM of target, as expected according to above estimation for antigen and antibody densities. Assuming a linear behavior at low target concentrations the electrochemical assays showed a sensitivity of $1.75 \pm 0.2\ \mu A\ nM^{-1}$ ($r^2 = 0.997$) in the range of 10–50 nM with LOD of 490 pM, respectively (Fig. 7).

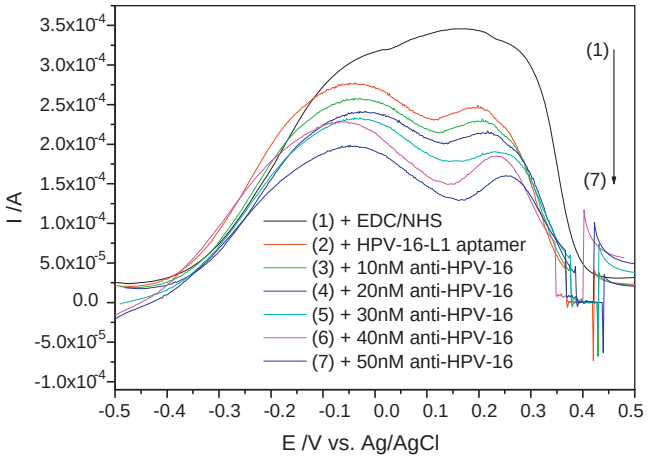

Fig. 6. SWV of PANi–MWCNT IDA recorded in HCl 0.1 M after treatment with EDC/NHS (curve 1), after grafting of 5×10^{-8} M HPV-16-L1 (curve 2) and after complexation with 10–50 nM of anti-HPV-16 (curves 3–7).

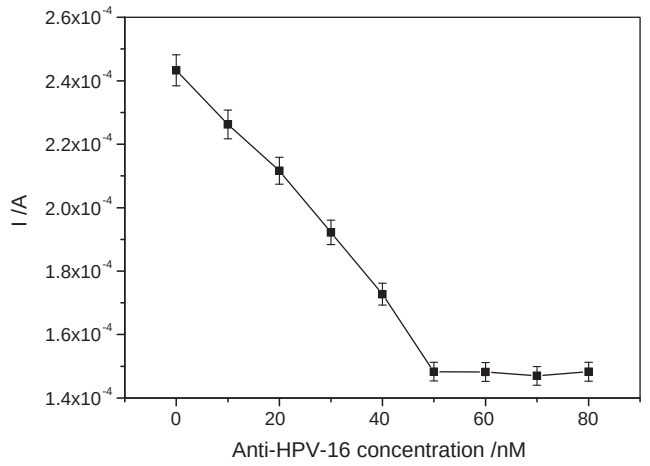

Fig. 7. The response curves of immunosensor with anti-HPV-16 concentration range from 0 to 80 nM.

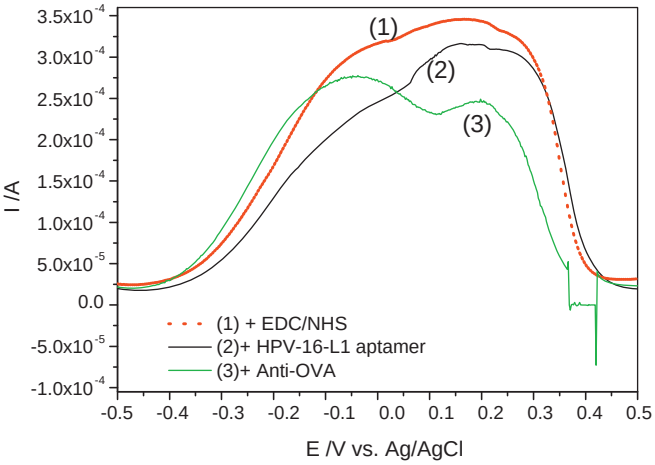

Fig. 8. SWV of PANi–MWCNT IDA recorded in HCl 0.1 M after treatment with EDC/NHS (curve 1), after grafting of 5×10^{-8} M HPV-16-L1 (curve 2) and after complexation with 5×10^{-8} M anti-OVA (curve 3).

Control experiments were also performed to confirm whether above signal decrease was really come from true complexation but not any other interfering phenomena like non-specific adsorption or signal instability. Thus, blank experiments were carried out with an irrelevant antibody directed against OVA (anti-OVA), whose molecular weight was 400 kDa, i.e. bigger than that of anti-HPV-16. As shown in Fig. 8, no complex formation (no signal drop) was observed for anti-OVA and HPV-16-L1. Another unspecific antibody (anti-KLH) has also shown the same results (figure not shown). In summary these experiments demonstrated clearly that the signal change was due to specific recognition by anti-HPV-16 antibody when complexing with HPV-16-L1 peptide aptamer.

4. Conclusion

Analytical performance of PANi–MWCNT based IDA arrays was evaluated. The assays showed a sensitivity of $1.75 \pm 0.2\ \mu A\ nM^{-1}$

($r^2 = 0.997$) in the range of 10–50 nM of anti-HPV with LOD of 490 pM. With concentration of or above 80 nM the SWV signal tends to saturation, as expected according to the theoretical estimation for antigen peptide aptamer (Ag) and Ab densities on the electrode surface. Control experiments with irrelevant antibodies (anti-OVA and anti-KLH) also confirmed that the signal decrease was really come from true complexation between Ag and Ab but not any other interfering phenomena like non-specific adsorption or signal instability.

One powerfully advantageous aspect of our arrays is the ability to array multiple copies of the same probes (to control for technical variability) as well as to array multiple probes against the same target on each electrode of IDA (to control for biological variability). With the functional conducting PANi–MWCNT immobilized Ag peptide aptamers as affinity capture reagent the concept of the reagentless electrochemical immunoarrays was proposed. As for the transduction scheme, it can proposed that the specific formation of Ag/Ab complex could be detected via change in signal transduction due to a steric hindrance, intervening in ion transport rate at the polymer–solution interface and therefore affects the redox behavior of PANi–MWCNT composite. Further work will be required to determine whether above described assays offer sufficient sensitivity and specificity for clinical use.

Acknowledgements

Funding of this work was mainly provided by Vietnam National Foundation for Science and Technology Development NAFOSTED grant (code 104.03-2010.60). Additional logistic support was also provided from MOST grant (code 59/2615/2010/HĐ-NĐT). We also acknowledge Prof. M.C. Pham and B. Piro (ITODYS, University of Paris Diderot, France) for initial suggestion and invaluable discussion regarding HPV choice as a model for Ab-Ag interaction study. The technical support of IMS-VAST key laboratory was critical for development and characterization of IDA.

References

[1] J. Ferlay, H.R. Shin, F. Bray, D. Forman, C. Mathers, D.M. Parkin, Estimates of worldwide burden of cancer in 2008: GLOBOCAN 2008, International Jounal of Cancer 127 (2010) 2893–2917.
[2] H.H. Handsfield, Clinical presentation and natural course of anogenital warts, The American Journal of Medicine 102 (1997) 16–20.
[3] F.X. Bosch, M.M. Manos, N. Muñoz, M. Sherman, A.M. Jansen, J. Peto, M.H. Schiffman, V. Moreno, R. Kurman, K.V. Shan, Prevalence of human papillomavirus in cervical cancer: a worldwide perspective, Journal of the National Cancer Institute 87 (1995) 796–802.
[4] C.E. Greer, C.M. Wheeler, M.B. Ladner, K. Beutner, M.Y. Coyne, H. Liang, A. Langenberg, T.S. Yen, R. Ralston, Human papillomavirus (HPV) type distribution and serological response to HPV type 6 virus-like particles in patients with genital warts, Journal of Clinical Microbiology 33 (8) (1995) 2058–2063.
[5] S. Laurensona, M.R. Petta, K. Hoppe-Seylerb, C. Denkb, F. Hoppe-Seylerb, N. Colemana, P. Ko Ferrigno, Development of peptide aptamer microarrays for detection of HPV-16 oncoproteins in cell extracts, Analytical Biochemistry 410 (2011) 161–170.
[6] M. Steben, E.D. Franco, Human papillomavirus infection: epidemiology and pathophysiology, Gynecologic Oncology 107 (2007) S2–S5.
[7] E.F. Dunne, E.R. Unger, M. Sternberg, G. McQuillan, D.C. Swan, S.S. Patel, L.E. Markowitz, Prevalence of hpv infection among females in the United States, The Journal of the American Medical Association 297 (2007) 813–819.
[8] A.R. Kreimer, G.M. Clifford, P. Boyle, et al., Human papillomavirus types in head and neck squamous cell carcinomas worldwide: a systematic review, Cancer Epidemiology, Biomarkers & Prevention 14 (2005) 467–475.
[9] J. Dillner, The serological response to papillomaviruses, Seminars in Cancer Biology 9 (1999) 423–430.
[10] S. Nagao, M. Yoshinouchi, Y. Miyagi, A. Hongo, J. Kodama, S. Itoh, T. Kudo, Rapid and sensitive detection of physical status of human papillomavirus type 16 DNA by quantitative real-time PCR, Journal of Clinical Microbiology 40 (2002) 863–867.
[11] S.D. Vernon, D.H. Farkas, E.R. Unger, V. Chan, D.L. Miller, Y.P. Chen, G.F. Blackburn, W.C. Reeves, Bioelectronic DNA detection of human papillomaviruses using eSensor™: a model system for detection of multiple pathogens, BMC Infectious Diseases 3 (2003) 12.
[12] N. Zari, A. Amine, M.M. Ennaji, Label-free DNA biosensor for electrochemical detection of short dna sequences related to human papilloma virus, Analytical Letters 42 (2009) 519–535.
[13] L. Civit, A. Fragoso, C.K. O'Sullivan, Electrochemical biosensor for the multiplexed detection of human papillomavirus genes, Biosensors & Bioelectronics 26 (2010) 1684–1687.
[14] L. Yang, X. Ren, F. Tang, L. Zhang, A practical glucose biosensor based on Fe_3O_4 nanoparticles and chitosan/nafion composite film, Biosensors and Bioelectronics 25 (2009) 889–895.
[15] J. Huang, G. Yanga, W. Meng, L. Wu, A. Zhu, X. Jiao, An electrochemical impedimetric immunosensor for label-free detection of *Campylobacter jejuni* in diarrhea patients' stool based on O-carboxymethylchitosan surface modified Fe3O4 nanoparticles, Biosensors and Bioelectronics 25 (2010) 1204–1211.
[16] P. Yáñez-Sedeño, J.M. Pingarrón, J. Riu, F. Xavier Rius, Electrochemical sensing based on carbon nanotubes, Trends in Analytical Chemistry 29 (2010) 939–953.
[17] B. Piro, A. Kapella, V.H. Le, G. Anquetin, Q.D. Zhang, S. Reisberg, V. Noel, L.D. Tran, H.T. Duc, M.C. Pham, Detection of human papilloma virus (HPV) infection by reagentless electrochemical peptide biosensor, Electrochimica Acta, (2011), doi:10.1016/j.electacta.2011.04.094, in press.
[18] P.J. Conroy, S. Hearty, P. Leonard, R. O'Kennedy, Antibody production, design and use for biosensor-based applications, Seminars in Cell & Developmental Biology 20 (2009) 10–26.
[19] E. Katz, I. Willner, Probing biomolecular interactions at conductive and semiconductive surfaces by impedance spectroscopy: routes to impedimetric immunosensors, DNA-sensors, and enzyme biosensors, Electroanalysis 15 (2003) 913–947.
[20] P. Holliger, P.J. Hudson, Engineered antibody fragments and the rise of single domains, Nature Biotechnology 23 (2005) 1126–1136.
[21] S. Wang, E.S. Humphreys, S.Y. Chung, D.F. Delduco, S.R. Lustig, H. Wang, K.N. Parker, N.W. Rizzo, S. Subramoney, Y.M. Chiang, A. Jagota, Peptides with selective affinity for carbon nanotubes, Nature Materials 2 (2003) 196–200.
[22] M. Yemini, M. Reches, Ehud Gazit, Judith Rishpon, Peptide nanotube-modified electrodes for enzyme-biosensor applications, Analytical Chemistry 77 (2005) 5155–5159.
[23] P. Samuelson, E. Gunneriusson, P.A. Nygren, S. Ståhl, Display of proteins on bacteria, Journal of Biotechnology 96 (2002) 129–154.
[24] A.J. Bard, L.R. Faulkner, Electrochemical Methods: Fundamentals and Applications, 2001.